SANDIA REPORT

SAND2015-8958
Unlimited Release
Printed October, 2015

Numerical Simulations of the Kolsky Compression Bar Test

Edmundo Corona

Prepared by
Sandia National Laboratories
Albuquerque, New Mexico 87185 and Livermore, California 94550

Sandia National Laboratories is a multi-program laboratory managed and operated by Sandia Corporation, a wholly owned subsidiary of Lockheed Martin Corporation, for the U.S. Department of Energy's National Nuclear Security Administration under contract DE-AC04-94AL85000.

Sandia National Laboratories

Issued by Sandia National Laboratories, operated for the United States Department of Energy by Sandia Corporation.

Available to DOE and DOE contractors from
U.S. Department of Energy
Office of Scientific and Technical Information
P.O. Box 62
Oak Ridge, TN 37831

Telephone: (865) 576-8401
Facsimile: (865) 576-5728
E-Mail: reports@adonis.osti.gov
Online ordering: http://www.osti.gov/bridge

Available to the public from
U.S. Department of Commerce
National Technical Information Service
5285 Port Royal Rd
Springfield, VA 22161

Telephone: (800) 553-6847
Facsimile: (703) 605-6900
E-Mail: orders@ntis.fedworld.gov
Online ordering: http://www.ntis.gov/help/ordermethods.asp?loc=7-4-0#online

SAND2015-8958
Unlimited Release
Printed October, 2015

Numerical Simulations of the Kolsky Compression Bar Test

Edmundo Corona
Sandia National Laboratories
PO Box 5800
Mail Stop 0840
Albuquerque, NM 87185

Abstract

The Kolsky compression bar, or split Hopkinson pressure bar (SHPB), is an experimental apparatus used to obtain the stress-strain response of material specimens at strain rates in the order of 10^2 to 10^4 1/s. Its operation and associated data reduction are based on principles of one-dimensional wave propagation in rods. Second order effects such as indentation of the bars by the specimen and wave dispersion in the bars, however, can significantly affect aspects of the measured material response. Finite element models of the experimental apparatus were used here to demonstrate these two effects. A procedure proposed by Safa and Gary (2010) to account for bar indentation was also evaluated and shown to improve the estimation of the strain in the bars significantly. The use of pulse shapers was also shown to alleviate the effects of wave dispersion. Combining the two can lead to more reliable results in Kolsky compression bar testing.

Acknowledgment

This project arose in discussions with Bo Song regarding optimal design of Kolsky bar testing, the accuracy of the acquired data, and how numerical simulations could help to improve both of these aspects. Bo was able to secure funding for the efforts presented in this report, and we have had many interesting discussions throughout the course of the project. Bo's many contributions are acknowledged with thanks. Thanks also go to Justin Crum, student intern at Sandia during the summer of 2015 and Brett Sanborn of the Shock Laboratory in Building 860 for many useful discussions regarding the finite element models and details of the experiments, respectively. Contributions by Erik Nishida to prepare some of the material in this report for a conference presentations are also acknowledged. Finally, the financial support by the WSEAT program, managed by Dennis Croessmann and David Epp, is acknowledged with thanks.

Contents

Appendix

Figures

Tables

Nomenclature

A	Cross-sectional area of bars
A_s	Cross-sectional area of specimen
E	Young's modulus
E_t^p	Plastic tangent modulus
L_s	Length of specimen
L_1	Length of striker
V_1	Initial velocity of striker
a, b	Distances from specimen to strain measuring points in bars
c_o	Wave speed from one-dimensional analysis
r	Radial coordinate
t, t_i, t_r, t_t, t_s	Time
u	Axial displacement
x	Axial coordinate
ε	Uniaxial strain in bars
$\varepsilon_i, \varepsilon_r, \varepsilon_t$	Incident, reflected and transmitted strain signals
ε_t^p	True plastic strain
ε_s	Uniaxial strain in specimen
ν	Poisson's ratio
ρ	Density
σ	Uniaxial stress in bars
σ_o	Yield stress
σ_s	Uniaxial stress in specimen
σ_t	True stress

1 Introduction

The Kolsky bar, also known as the split Hopkinson bar (Chen and Song, 2011), is an experimental apparatus used to test materials at high strain rates, usually in the order of 10^2 to 10^4 1/s. Different designs have been used to load material specimens in compression or in tension. Figure 1(a) shows a schematic of the basic compression apparatus. The material specimen is sandwiched between two long metal bars as shown. A third bar, the striker, impacts the bar on the left, which is called the incident bar, axially with velocity V_1 as shown.

The impact sends a stress pulse (incident pulse) that travels down the bar. Strain gages at location 1 in the bar sense the axial strain generated by the pulse. Figure 1(b) schematically shows the strain signal as ε_i as would be seen in a strain-time record. When the pulse arrives at the location of the specimen, a portion is reflected (reflected pulse) while another portion is transmitted (transmitted pulse) through to the transmission bar. During this process, the right end of the incident bar moves to the right more than the left end of the transmission bar, thus compressing the specimen. Strain gages at location 2, on the transmission bar, measure the axial strain generated by the passing transmitted pulse, labeled ε_t in Fig. 1(b), while strain gages at location 1 sense the strain ε_r due to the reflected pulse. As will be shown in the next section, the stress and strain in the specimen can be determined based on the strain measured at the two gage locations using results from wave propagation theory in rods.

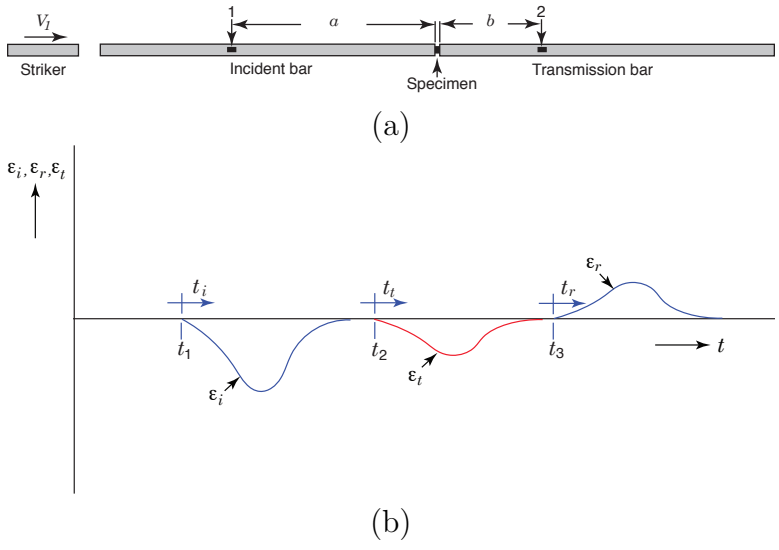

Figure 1. (a) Schematic of the Kolsky compression test set-up and (b) schematic of strain gage signals.

Although the theory of one-dimensional stress wave propagation in rods yields the necessary relations to determine the stress and strain in the specimen, some second order effects

can influence the measurements and therefore distort the specimen's stress-strain relation obtained from the test. In the current work, finite element models of the Kolsky bar are used with the objective of demonstrating the influence of such second order effects, and also to study proposed methods to compensate for them.

The method to be used is based on the premise that since the specimen material properties are prescribed in the model, one would expect that the uniaxial stress-strain curve extracted from the test simulation should agree with the one that was input. So, provided that the fidelity of the finite element model is sufficient, differences between the prescribed and calculated uniaxial stress-strain responses are indicators of effects unaccounted for in the data reduction process.

2 Basic One-Dimensional Stress Wave Propagation Theory for the Kolsky Bar

The functioning of the Kolsky bar can be understood from the basic theory of wave propagation in slender rods. In fact, the reduction of data to determine the response of the specimen is based on the results of this theory. The formulation and solutions of the wave equation in rods have been presented in books such as those by Graf (1975) and Kolsky (1953). The basic concepts will be reviewed first to set the stage for later discussion of the limitations that using this theory puts on the analysis of compression tests and also of some remedies used to compensate for them.

2.1 Basic Solutions for Wave Propagations in Rods

Consider a prismatic slender rod of cross-sectional area A made with a linearly elastic material with density ρ and Young's modulus E as shown in Fig. 2. The coordinate along the axis of the rod is x and the axial displacement of particles in the rod is given by u, which is taken to be uniform over the cross-section. Suppose that the rod has been excited dynamically such that at a given time t it contains a propagating disturbance that has a uniaxial stress (σ) distribution somewhere along its length as shown in the figure. Although the stress distribution varies along the length of the bar, it is constant over the cross-section at any given x, as required by the similar statement made for u. At this point it suffices to say that the bar can be considered to be slender if the stress distribution is relatively smooth and has a length that is significantly larger than the cross-sectional dimensions of the bar.

To aid in the derivation of the equation of motion, the free-body diagram of a bar segment of length dx is also shown in the figure. Applying Newton's second law gives

$$\frac{\partial \sigma}{\partial x} = \rho \frac{\partial^2 u}{\partial t^2}. \tag{1}$$

Using Hooke's law, $\sigma = E\varepsilon$ where $\varepsilon = \frac{\partial u}{\partial x}$ is the axial strain, and substituting into (1) gives the wave equation

$$\frac{\partial^2 u}{\partial x^2} = \frac{1}{c_o^2} \frac{\partial^2 u}{\partial t^2} \tag{2}$$

where

$$c_o = \sqrt{\frac{E}{\rho}}. \tag{3}$$

Note that the governing equation (2) is linear. This useful fact implies that the principle of superposition is valid.

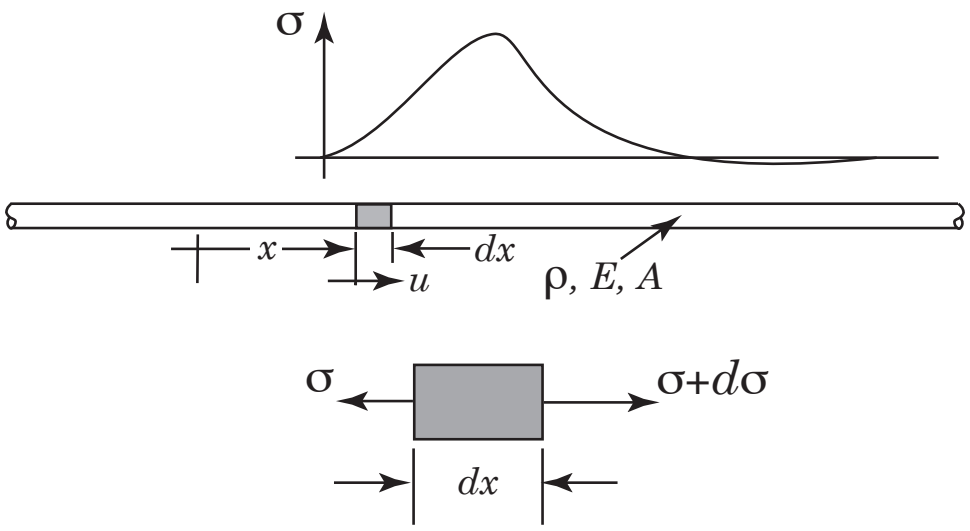

Figure 2. Schematic at time t of a slender rod with a stress distribution and free body diagram of an infinitesimal rod element.

A solution[1] of (2) is given by

$$u(x,t) = f(x - c_o t) + g(x + c_o t). \tag{4}$$

Since f is a function of $x - c_o t$, then as t increases x must increase as well thus indicating that f translates towards larger values of x without changing shape. Considering $x - c_o t =$ constant gives that $dx = c_o dt$ thus indicating that c_o is the velocity at which the disturbance moves and is called the *wave speed*. The function g has similar characteristics but moves in the opposite direction.

Once the expression for the particle displacement u is known, other quantities of interest such as the particle velocity v, the axial strain ε and the axial stress σ in the bar can be easily found for any x and t. It is customary to let $f' = \frac{df}{d(x - c_o t)}$ and $g' = \frac{dg}{d(x + c_o t)}$. Then the expressions for the quantities of interest are:

$$v(x,t) = \frac{\partial u}{\partial t} = -c_o f' + c_o g', \tag{5}$$

$$\varepsilon(x,t) = f' + g' \tag{6}$$

and

$$\sigma(x,t) = E(f' + g') \tag{7}$$

[1] D'Alembert's solution, 1747.

Two important cases that directly relate to the workings of the Kolsky bar test need to be considered: impact between two bars and reflection/transmission at impedance (defined as EA/c_o) discontinuities. Before considering these two cases, however, it is necessary to also consider the reflection of a wave from the free end of a bar. Appendix A shows the solutions to these cases. For the purposes at hand, however, it is sufficient to only present the final results:

- A stress pulse reflects off a free end with the same shape and magnitude, but with opposite sign.
- Axial impact between an initially moving bar (striker) of length L_1 traveling with velocity V_1 and a stationary long bar causes a compressive rectangular stress pulse to propagate down the long bar while the striker stops moving and finishes stress free. The magnitude of the stress pulse is given by $\sigma = EV_1/2c_o$, the spatial length of the pulse is $2L_1$ and the temporal length is $\frac{2L_1}{c_o}$.
- When a pulse propagating in a bar reaches an impedance discontinuity, part of the pulse is transmitted and part is reflected.

2.2 Analysis of the Kolsky Bar

Looking back at Fig. 1, let t_1 and t_3 be the times at which the incident and the reflected pulses, respectively, reach location 1 in the incident bar. Also let t_2 be the time at which the transmitted pulse reaches location 2 in the transmission bar. It is important to make the distance a in Fig. 1 long enough to first see the incident pulse pass completely and then, at a later time, see the reflected pulse do the same. In other words, the incident and reflected pulses should not be active simultaneously at location 1.

Define the time variables t_i, t_t and t_r as indicated in Fig. 1(b) in terms of t such that

$$\begin{aligned} t_i &= \langle t - t_1 \rangle \\ t_t &= \langle t - t_2 \rangle \\ t_r &= \langle t - t_3 \rangle \end{aligned} \tag{8}$$

where $\langle\rangle$ are Macaulay brackets defined as

$$\langle t \rangle = \begin{cases} 0, & t < 0 \\ t, & t \geq 0 \end{cases} . \tag{9}$$

The times t_1, t_2 and t_3 are the times at which the incident, transmitted and reflected pulses arrive at the strain gage locations. Given the distances a and b in Fig. 1(a) and the wave

propagation speed c_o, t_2 and t_3 can be defined in terms of these parameters and t_1 as follows:

$$\begin{aligned} t_2 &= t_1 + \frac{a+b}{c_o} \\ t_3 &= t_1 + \frac{2a}{c_o}. \end{aligned} \tag{10}$$

In addition, define another time variable t_s as

$$t_s = \langle t - t_4 \rangle \tag{11}$$

where

$$t_4 = t_1 + \frac{a}{c_o} \tag{12}$$

is the time at which the incident pulse reaches the location of the specimen.

From equation (6) we have that at the interface between the incident bar and the specimen

$$\varepsilon(t_s) = f' + g' = \varepsilon_i(t_i) + \varepsilon_r(t_r) \tag{13}$$

and that, from (5)

$$v(t_s) = -c_o f' + c_o g' = c_o \left[-\varepsilon_i(t_i) + \varepsilon_r(t_r) \right]. \tag{14}$$

Therefore, the displacement of this end of the incident bar, u_i^s is given by

$$u_i^s(t_s) = c_o \left[\int_0^{t_i} -\varepsilon_i \, d\tau + \int_0^{t_r} \varepsilon_r \, d\tau \right]. \tag{15}$$

Looking at the transmission bar next, let the bar be long enough such that only the rightward-traveling function will have to be considered. Following arguments similar to those used for the incident bar yields

$$u_t^s(t_s) = -c_o \int_0^{t_t} \varepsilon_t \, d\tau. \tag{16}$$

The engineering strain in the specimen is then given by

$$\varepsilon_s(t_s) = \frac{u_t^s(t_s) - u_i^s(t_s)}{L_s} \tag{17}$$

where L_s is the length of the specimen. Therefore, substituting (15) and (16) into (17) gives the engineering strain in the specimen.

The load on the specimen can also be determined from the strains measured at the gages. From (7) the stress in the incident bar is

$$\sigma(t_s) = E(f' + g') = E\left[\varepsilon_i(t_i) + \varepsilon_r(t_r)\right], \tag{18}$$

so the load at the interface between the incident bar and the specimen P_i is given by

$$P_i(t_s) = EA\left[\varepsilon_i(t_i) + \varepsilon_r(t_r)\right]. \tag{19}$$

Similarly, the load at the interface between the transmission bar and the specimen P_t is given by

$$P_t(t_s) = EA\varepsilon_t(t_t). \tag{20}$$

Assuming that the specimen is in a state of equilibrium such that $P_i = P_t$ and therefore $\varepsilon_t(t_t) = \varepsilon_i(t_i) + \varepsilon_r(t_r)$, then from (15) and (16) and (17), the strain in the specimen is given in terms of ε_r as follows

$$\varepsilon_s(t_s) = -\frac{2c_o}{L_s}\int_0^{t_r} \varepsilon_r \, d\tau. \tag{21}$$

and the stress in the specimen can be obtained from

$$\sigma_s(t_s) = \frac{A}{A_s} E\varepsilon_t(t_t), \tag{22}$$

where A_s is the cross-sectional area of the specimen.

3 Finite Element Analysis of the Kolsky Bar Test

3.1 Finite Element Model

Figure 3 shows a sketch of the geometry of the model that will be used to conduct the numerical simulations. All bars have circular cross-section with diameter of 0.75 in. The striker has a length of 12 in. while the incident and transmission bars have a common length of 144 in. The specimen is a short circular cylinder with length and diameter of 1/8 and 1/4 in. respectively. The axial strains in the bars are monitored at locations 1 and 2 that are 40 in. from the bar/specimen interface as shown. All components of the model are initially at rest, with the exception of the striker, which has an initial velocity V_1.

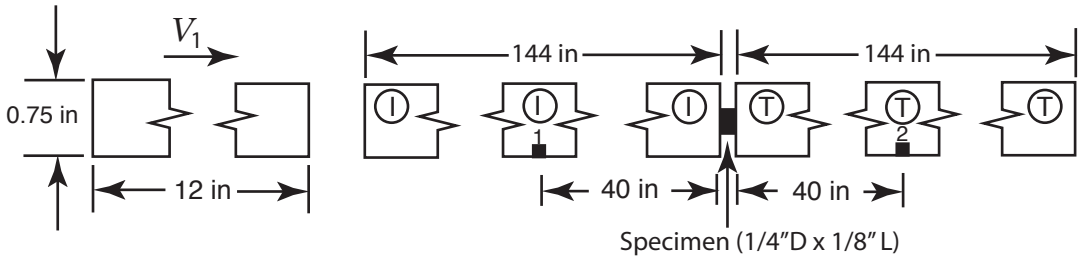

Figure 3. Geometry of the model.

All bars are linearly elastic with density ρ, Young's modulus E and Poisson's ratio ν. The specimen is taken to be a rate-independent elastic-plastic solid that hardens isotropically and has yield stress σ_o and a bilinear true stress-strain curve with plastic tangent modulus E_t^p. Table 1 lists the material properties of the baseline model.

Table 1. Material properties for baseline model.

	ρ (slug-ft/in^4)	E (ksi)	ν	σ_o (ksi)	E_t^p (ksi)
Bars	7.48×10^{-4}	30×10^3	0.3	-	-
Specimen	7.48×10^{-4}	30×10^3	0.3	40	450

The finite element model was developed within the commercial code Abaqus/Explicit Version 6.14 using four-node, reduced integration, continuum axisymmetric elements CAX4R. The element size was varied from 4 elements through the radius of the bars far away from the specimen to 24 through the radius near the specimen. For the most part the elements had unit aspect ratio, except in four small regions where the element sizes transitioned from one size to the next. Element size transitions had minimum effect on wave propagation. The specimen had constant element size with 8 elements through the radius.

3.2 Results

The numerical simulations were conducted by taking $V_1 = 267$ in/s. Based on the results discussed in Section 2.1 this gives rise to a 20 ksi square stress incident pulse, corresponding to a strain of 6.7×10^{-4} in the incident bar. The length of the pulse would be 24 in. and the transit time 0.12 ms. Figure 4 shows the strain traces obtained at the location in the two bars where they were monitored. They are shown as a function of t, where $t = 0$ when the striker first impacts the transmission bar. The blue line corresponds to location 1 while the red trace corresponds to location 2. Looking at the incident strain pulse ε_i shows that it has approximately the correct amplitude and duration. The oscillatory nature of the pulse is due to dispersion effects in the bar induced by the effect of radial inertia (see chapter 2 in Graff, 1975). Since the distances from the specimen to the strain monitoring locations in both bars are the same, the reflected pulse ε_r in the incident bar and the transmitted pulse ε_t in the transmssion bar arrive at the same time at the respective locations.

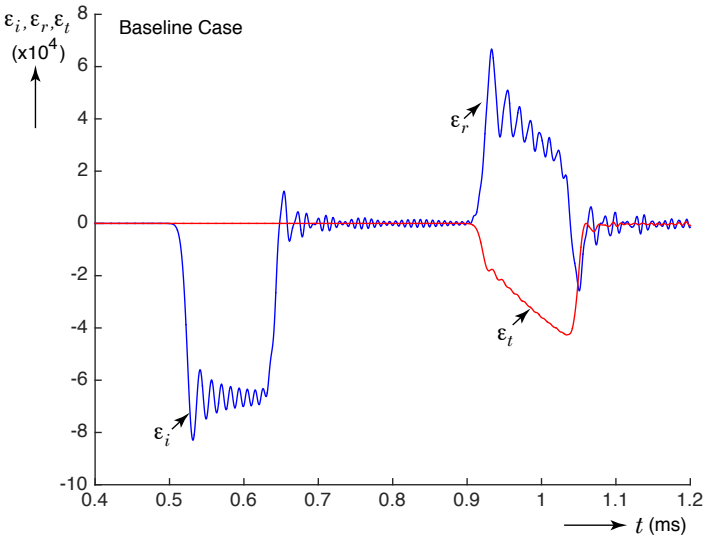

Figure 4. Incident and transmission bar strains measured 40 in. away from the specimen in the baseline case.

Using Equations (15) and (16) to calculate the displacements of the bars at the specimen ends and then (17) gives the engineering strain in the specimen, ε_s. In addition, (22) gives the engineering stress in the specimen, σ_s. The calculated stress-strain curve is shown in Fig. 5(a)[2]. The expected engineering stress-strain curve based on the parameters in Table 1 is shown in dashed line and labeled 'Target.' Ideally, the calculated curve should coincide with the target. It, however, does not, and two observations stand out:

1. The slope of the elastic region is significantly underestimated by the calculations, and

[2]Calculating ε_s using (21) gave essentially the same curve

the calculated curve also lies below the target in the plastic range.

2. The calculated curve displays oscillatory behavior.

Figure 5(b) shows the calculated engineering strain rate in the specimen $\dot{\varepsilon}_s$ as a function of t_s. Clearly, the strain rate shows an oscillatory behavior during the loading of the specimen and its mean gradually decreases from about 1500 to about 800 1/s during the test. Ideally $\dot{\varepsilon}_s$ should be constant since usually the material response at a given strain rate is desired.

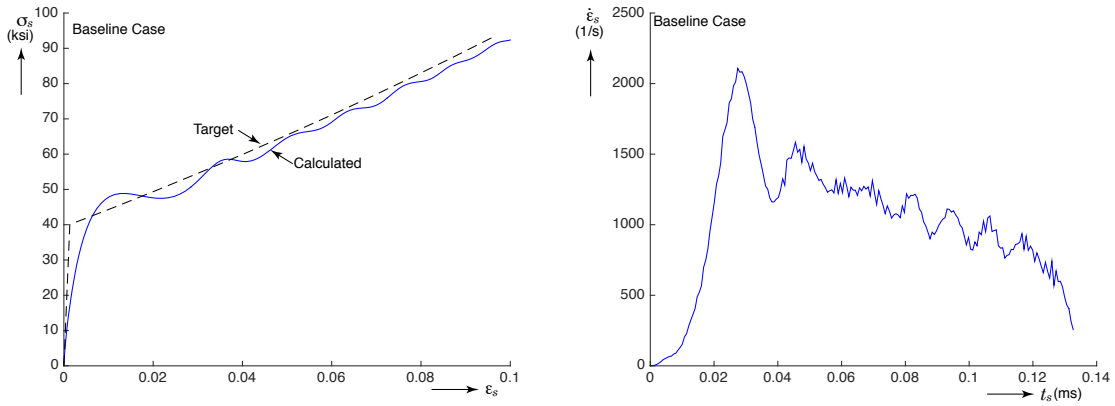

(a) (b)

Figure 5. Results for the baseline case. (a) Comparison of engineering stress-strain curve calculated via Eqns. (15) to (17) and (22) against the target curve, and (b) engineering strain rate calculated for the baseline case.

To explain the reason that the slope of the elastic region is underestimated by the standard Kolsky bar data reduction, and similarly the stress-strain curve is below the target, it is necessary to investigate the deformation of the bars and the specimen at their interfaces. Figure 6(a) shows the displacement of the incident bar/specimen interface, while Fig. 6(b) shows the same for the transmission bar/specimen interface. The bar profiles are shown in blue line whereas the specimen profiles are shown in red. Each set of profiles corresponds to a given σ_s as indicated by the labels.

The penalty contact method was used to handle contact between all surfaces that interacted in the model. The default penalty stiffness had to be scaled by a factor of 10 in order to bring the interpenetration at the bar/specimen interfaces to an acceptable value. This caused a reduction in the time increment in the explicit procedure but given the relatively small size of the model it did not result in inordinate increases in run time. All contact in the model was taken to be frictionless.

The most notable aspect shown in Fig. 6 is the indentation by the specimen of the bar surfaces. Clearly, plane sections do not remain plane at the ends of the bars and the specimen

as assumed by the one-dimensional wave propagation theory used in the calculation of the stress-strain curve in Fig. 5(a). In fact, the calculated bar displacements using Equations (15) and (16) are shown in black dashed lines. Note that the dashed lines overestimate the axial displacement of the specimen at the incident side and underestimate it at the transmitted side thus overestimating the compression of the specimen and hence the compressive axial strain. This overestimation of the specimen strain is one important reason of why the modulus of elasticity appears smaller than expected and the calculated curve falls below the expected results in Fig. 5(a).

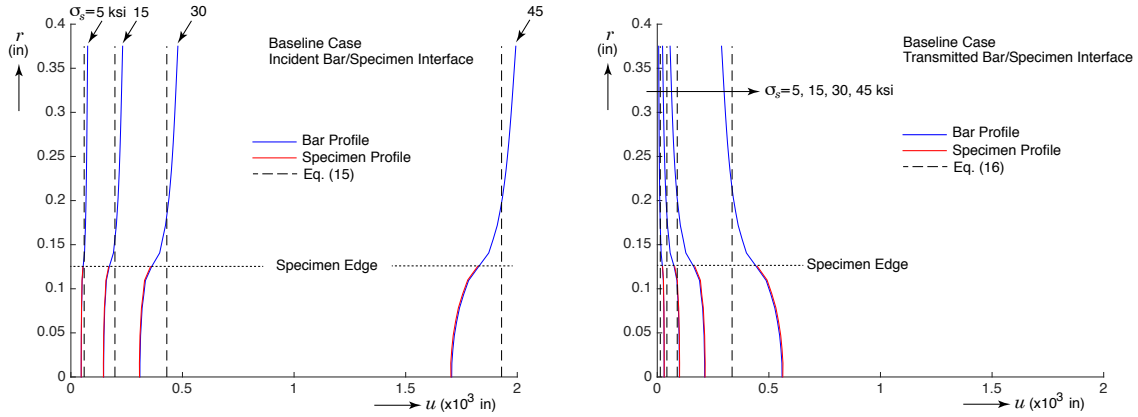

Figure 6. Comparison between the bar and specimen profiles determined from the finite element calculations and the plane profiles calculated from Equations (15) and (16). (a) At the interface between the incident bar and the specimen and (b) at the interface between the specimen and the transmission bar.

Another obvious aspect apparent in Fig. 6 is that the displacement of the incident bar end is much larger than that of the transmission bar, which enables the compression of the specimen. Also note that the shape of the indentation of the bars appears to be more rounded for the 45 ksi profiles than the other three. This has to do with the transition from elastic to plastic deformation of the specimen material. Finally, since the specimen surfaces are not plane, its state of deformation is not strictly uniform. Figure 7 shows the axial logarithmic strain in the specimen when the engineering strain $\varepsilon_s = 5\%$. It exhibits a variation in the order of 8% within the bulk of the specimen with the largest strains being near the surface of the specimen where it contacts the bars.

In order to demonstrate that the indentation issue addressed above is indeed a large contributing factor to the differences between the calculated and the target stress-strain curves, Fig. 8(a) shows stress-strain curves calculated based on the contact forces at the interface and the displacement of the specimen at the interface. Two curves are shown: the one labeled ε_{sc} has the strain calculated from the relative displacements at the center of the

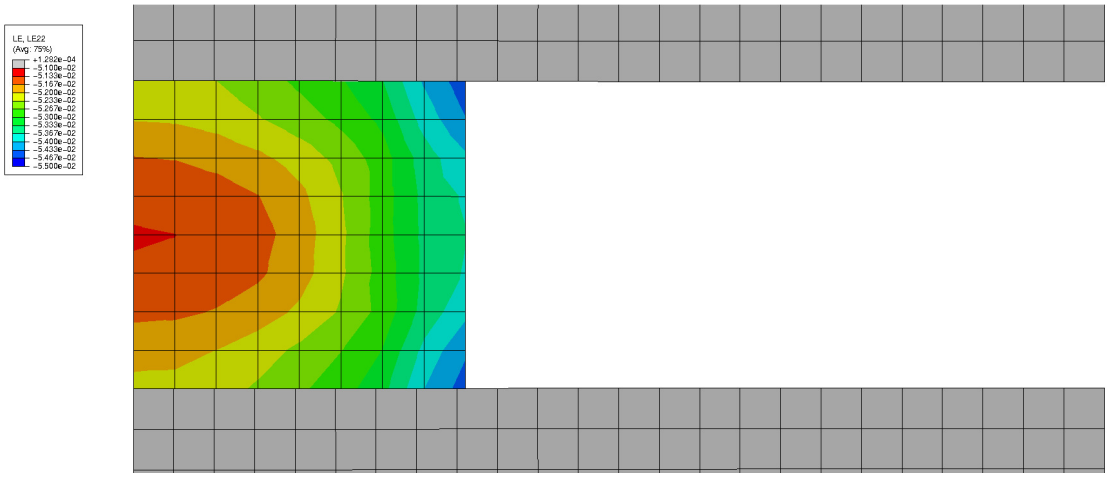

Figure 7. Axial logarithmic strain contours in the specimen when $\varepsilon_s = 0.05$ show a variation of about 8% across the specimen.

specimen while the other uses the relative displacements at the edge of the specimen, as shown in the insert. Figure 8(b) shows a zoomed view of the vicinity of the elastic region. Clearly, the stress-strain curves calculated in this manner are much closer to the target than the one calculated via Eqns. (15) to (17) and (22) in Fig. 5(a). It is also obvious that the strains calculated based on the center displacement are smaller than those calculated from the edge displacement. Note that the target is bounded by the two calculations. This method of calculating the stress-strain response of the specimen, however, is not available to the experimentalist.

More careful review of the finite element results showed that, as expected, the stress in the bars near the bar/specimen interfaces was not homogeneous within the cross-section. This stress inhomogeneity, however, was restricted to a length of a few bar radii. When the wave propagation signals reached the points where the bar strains were output, the stress was uniform over the cross-section. This is a manifestation of St. Venant's principle and represents a loss of information of what happened at the bar/specimen interface as the signal traveled from those sites to the monitored locations. It therefore appears that, from a practical point of view, more accurate estimates of the specimen stress-strain curve could be obtained if a method to estimate the indentation of the bars could be developed. On a final note, we observe that the amplitude of the stress oscillations in Fig. 8(a) is much smaller than that in Fig. 5(a). This may be attributed to dispersion effects and will be addressed later in the report.

In a relatively recent paper, Safa and Gary (2010) proposed a method to "provide a 3-D displacement correction for local punching due to axial load at the end of a bar." Their work was motivated by the indentation issue in Kolsky bars discussed above. In their paper they provided a method, based on linear elasticity, to correct the stress-strain curve obtained from

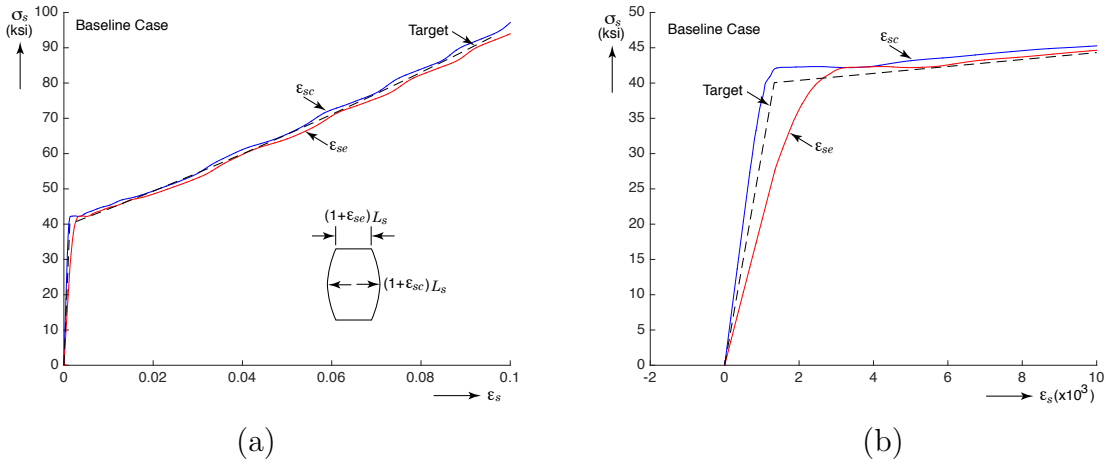

(a) (b)

Figure 8. Target and stress-strain curves calculated from the contact force between the incident bar and the specimen and the axial deformation of the specimen at the center or at the surface. (a) To 10% strain and (b) detail near the elastic range.

the bar strain data. In essence, the indentation of the bars is calculated as a linear function of the force between the bars and the specimen. Since the force is a measured quantity, it is relatively straightforward to calculate the bar indentation and correct the specimen stress-strain curve. Figure 9 shows the result of applying the indentation correction to the results in Fig. 5(a) by the line labeled 'S/G.' Overall, the corrected results lie closer to the target curve. Figure 9(b) shows a close up near the elastic region. Although the correction is closer to the target curve, the results are still somewhat unsatisfactory because of the high curvature of the results.

Safa and Gary provided guidance to understand this discrepancy. The first point they made was that the correction for the indentation is based on a state of motion at the interfaces that is free of transients. Their recommendation is to utilize the correction only for times larger that the time it takes for a full round trip of a surface wave from the center of the bar to the edge and back. For the case at hand, this is the time required for σ_s to raise about 10 ksi. Therefore the correction of the curve below 10 ksi, where the strain seems to be slightly negative, should not be considered valid. The second point that Safa and Gary make is that one must take into account the effect of dispersion in the bars when conducting the data reduction to obtain the specimen stress-strain curve. This latter consideration has not been implemented in the results shown.

The customary way of mitigating the effect of dispersion in the Experimental Impact Mechanics Laboratory (EIML) at Sandia is to place a thin metal disk at the site where the striker bar impacts the incident bar. This metal disk is commonly called a 'pulse shaper' because it modifies the shape of the pulse propagating through the incident bar. Another

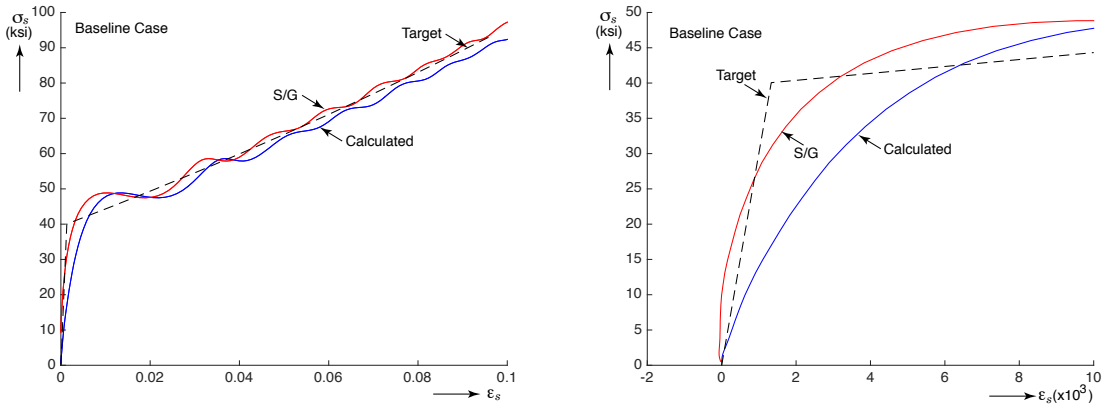

Figure 9. Comparisons bweteen the raw engineering stress-strain curve, the one corrected by Safa and Gary's method and the target. (a) To 10% strain and (b) detail near the elastic range.

function of the pulse shaper is to induce a more uniform strain rate in the specimen during loading.

In essence, the phenomenon of dispersion causes the different frequency components of the pulse to travel at different speeds, with high frequency signals propagating at speeds lower than c_o. For the bar material and dimensions at hand, signals with frequency above 120 kHz propagate with speeds that are under $0.95c_o$.

As far as dispersion is concerned, the effect of the pulse shaper is to cushion the impact between the striker and the incident bar, therefore eliminating high frequencies from the incident pulse, but also changing its shape, elongating its duration and diminishing its amplitude as demonstrated previously (Corona, 2014). As an example, consider a case where a copper pulse shaper with diameter and thickness of 0.25 and 0.040 in. is used. Everything else is exactly the same as in the baseline case. The properties of annealed copper C11000 are taken to be as shown in Table 2. The material is assumed to be a rate-independent elastic-plastic solid that hardens isotropically. Its hardening behavior was based on data provided by Song (2014). The true stress-plastic-strain pairs used to define the hardening behavior are given in Table 3.

Table 2. Physical properties used for annealed copper C11000.

ρ (slug-ft/in^4)	E (ksi)	ν
8.37e-4	16.e6	0.343

Table 3. True stress and true plastic strain pairs used to describe the hardening behavior of annealed copper C11000.

σ_t	ε_t^p
4830.	0
23465.	0.0498
36720.	0.1031
51840.	0.2199
69342.	0.3524
69960.	0.5064
75000.	0.6884

Figure 10 shows the strain traces at the monitoring locations using the same scales as in Fig. 4. Note that the pulse for ε_i is much cleaner with the pulse shaper, but the pulse period is longer and the magnitude of the strain is smaller. Also the shape of the pulse is closer to that of a triangular pulse than a square one. The reflected and transmitted pulse, ε_r and ε_t, also seem very clean.

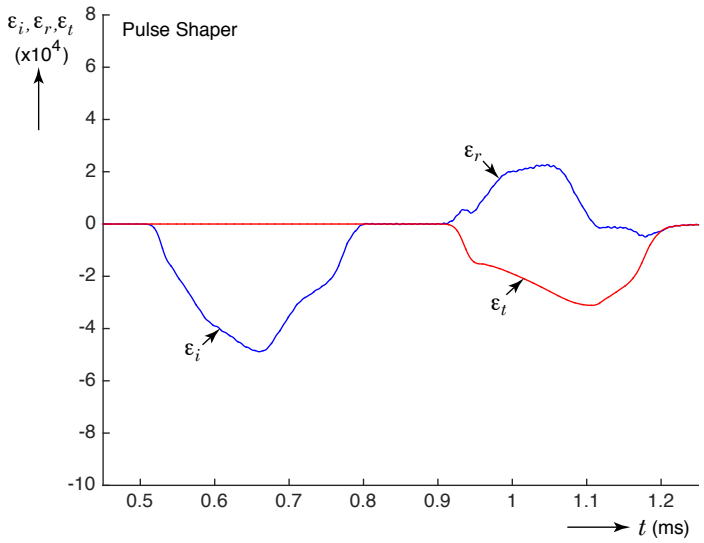

Figure 10. Incident and transmission bar strains measured 40 in. away from the specimen when a pulse shaper was included in the model.

Figure 11(a) shows comparisons of the specimen stress-strain curve calculated from Equations (17) and (22), the curve after applying the correction of Safa and Gary, and the target curve. Note that the oscillations have been nearly eliminated and that very good agreement is now seen between the curve corrected for indentation and the target. Figure 11(b) shows a

close up of the vicinity of the elastic region, and demonstrates that applying the indentation correction gives a very close estimate of Young's modulus as well as of the shape of the curve near the yield point. Finally, Fig. 11(c) shows that the strain rate during loading was nearly constant over about half of the time period and did not exhibit the large oscillations that were observed when the pulse shaper was not included. The strain rate achieved, however, was significantly less than when no pulse shaper was used. Finally note that elastic unloading occurred at a strain of about 8%. By contrast, without the pulse shaper the specimen strain reached 13% prior to unloading. So in order to reach higher strains when the pulse shaper is used would require a longer striker bar. Clearly, the design of pulse shapers has to be balanced depending on the test conditions desired such as strain rate, hardening behavior of the specimen material, extent of loading and reduction of dispersion effects. Numerical models such as those presented here should be able to provide guidance to zero in on a optimal test configuration for a given test material and conditions.

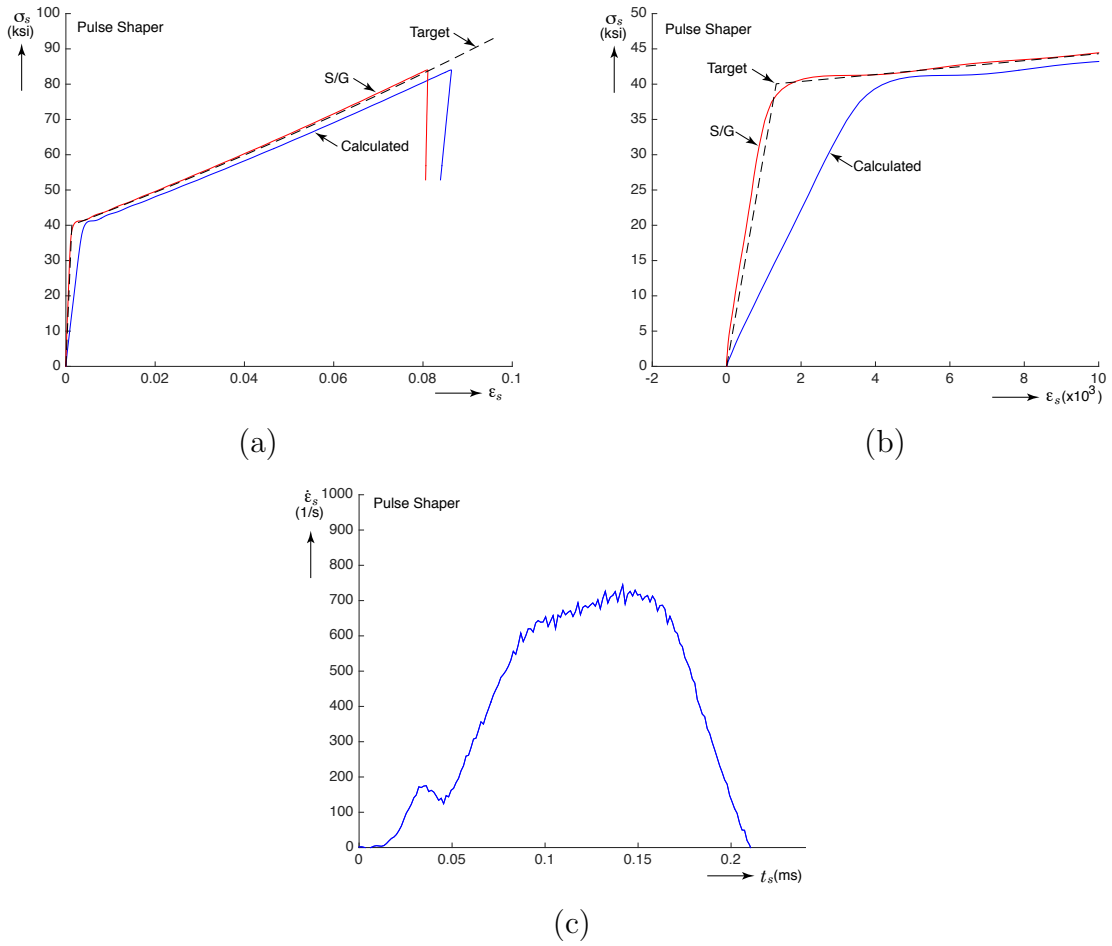

Figure 11. Results obtained when a copper pulse shaper of diameter and thickness 0.25 and 0.040 in. respectively was placed between the striker and the incident bar. (a) Comparison of the raw stress-strain curve, the one corrected by Safa and Gary's method, and the target, (b) detail near the elastic range and (c) calculated strain rate.

4 Summary and Conclusions

The work presented in this report consisted of conducting finite element simulations of the Kolsky bar test and then extracting data and reducing it in the same way that would have been done in an actual experiment to determine the stress-strain curve of a metal elastic-plastic specimen. Since the input stress-strain curve was known, it provided a simple way to evaluate the data reduction procedure by comparing the engineering stress-strain curve used in the input to that obtained from the data reduction procedure. The results showed that in order to obtain good agreement between the calculated and target stress-strain responses the correction suggested by Safa and Gary should be included. In addition, a way to control dispersion effects also needs to be implemented. In the calculations presented a pulse shaper was used for this purpose

The results also demonstrated the potential utility of numerical simulations of the experimental set-up to optimize test designs. It seems plausible that numerical simulations can be used to, for example, design pulse shapers, striker bars and specimen geometries that optimize the test design to achieve a given range of strain rates and ranges while maximizing the attenuation of dispersion effects.

References

Chen, W. and Song, B. 2011. Split Hopkinson (Kolsky) Bar. Design, Testing and Applications. Springer Science.

Corona, E. 2014. Numerical Simulations of Wave Propagation in Long Bars with Application to Kolsky Bar Testing. Memo to distribution. SAND2014-19397 R. Sandia National Laboratories, Albuquerque, NM.

Graff, K.F. 1975. Wave Motion in Elastic Solids. Oxford University Press and Dover Publications, Inc.

Kolsky, H. 1953. Stress Waves in Solids. Clarendon Press and Dover Publications, Inc.

Safa, K. and Gary, G. 2010. Displacement Correction for Punching at a Dynamically Loaded Bar End. *International Journal of Impact Engineering*, **37**, pp. 371–384.

Song, B. 2014. Personal communication.

A Solutions of the Wave Equation for Reflection from a Free End, Impact and Impedance Mismatch

Reflection from a Free End

Consider a compressive stress pulse of rectangular shape moving towards the right as shown in Fig. A.1(a) by the thick black line in the upper graph. The boundary condition at the free end is that σ must be zero. From (7) and (4) it can be deduced that u will have the shape shown in the lower graph. The red dashes also represent the stress and displacement functions as they travel rightward at this time. The end of the bar is indicated by the short vertical line. The zero stress condition at the end can be satisfied using the principle of superposition by imagining that the bar continues beyond the end, but also that a similarly shaped tensile stress pulse is propagating to the left as shown by the dashed green line. The distance to the end of the bar of both pulses is the same. The corresponding displacement function is also shown in green dashed line.

At a later time, the situation becomes as shown in Fig. A.1(b). The red functions have continued beyond the line indicating the boundary of the bar, whereas the green ones have entered the region of the bar. The sum of the two functions over the region of the bar, which actually represents the actual stress and displacement are shown in dark black line. The arrows indicate the direction of motion of the fronts. Note that the stress at the end of the bar is zero, and the region of zero stress is lengthening by propagating to the left. The displacement at the end of the bar is increasing. A little later, the situation is as shown in Fig. A.1(c). The region of zero stress is now shortening as the right edge of the now tensile stress front propagates to the right. The end displacement continues to increase at the same rate. Finally, Fig. A.1(d) shows the fully reflected pulse being tensile. The displacement is now constant behind the reflected front. In summary, at a free end compressive stress pulses reflect as tensile pulses and the displacement at the bar end increases by twice as much by the reflection of the pulse as points interior to the bar displace by the passage of a single pulse.

Impact Between Two Bars

Consider the longitudinal impact between two rods. In the scenario of interest, one of the rods (the striker) has finite length L_1 and is traveling to the right with speed V_1 while the other rod, denoted by 2, is semi-infinite and initially at rest. For simplicity, and as is often the case in Kolsky bar testing, let both bars have equal values of ρ, E and A. Let the impact start at $t = 0$ and the origin of the axial coordinate x be at the left edge of the striker. Impact between two rods is significantly more complicated to explain compared to the pulse reflection described previously. In this case, we will have to consider the functions $f(x,t)$ and $g(x,t)$ that appear in (4). To satisfy the initial conditions the expressions for f and g

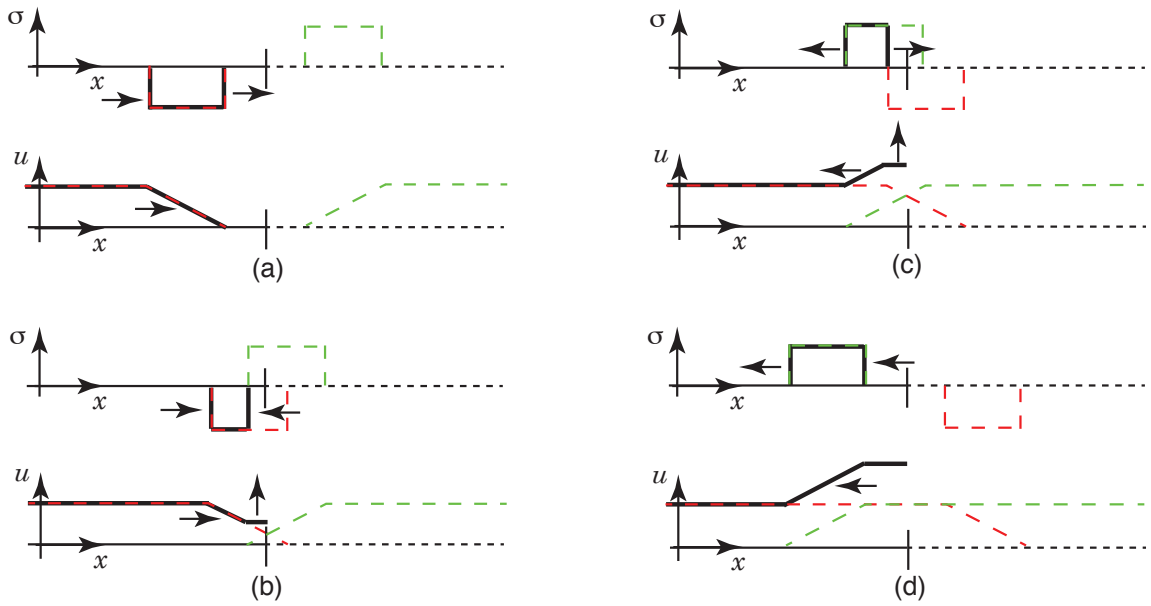

Figure A.1. Schematic showing the use of superposition to illustrate the reflection of a rectangular stress pulse at the free end of a bar. (a) As the pulse approaches the free end, (b) early part of the reflection, (c) late part of the reflection and (d) after the reflection.

are given by

$$
\begin{aligned}
f(x,0) &= \begin{cases} -\frac{V_1}{2c}x,\ 0 \le x < L_1 \\ -\frac{V_1}{2c}L_1,\ x \ge L_1 \end{cases} \\
g(x,0) &= \begin{cases} \frac{V_1}{2c}x,\ 0 \le x < L_1 \\ \frac{V_1}{2c}L_1,\ x \ge L_1 \end{cases}
\end{aligned} \tag{23}
$$

as shown in the top sketch in Fig. A.2(a). The resulting particle displacement is shown in black line. Recall that f moves to the right while g moves to the left as indicated by the arrows. The derivatives f' and g' are also shown in the lower two sketches. The particle velocity and the stress, shown in black line, are given in terms of these derivatives as shown in (5) and (7). The solutions in (23) give all particles in the striker bar a constant speed V_1 while the second rod is at rest and both bars are stress-free. Since the left end for the striker bar (at $x = 0$) is free we can again use superposition and introduce a fictitious function $\bar{f}$, shown in green and moving to the right, to satisfy the boundary condition $\sigma = 0$ at that location as was done in the previously discussed scenario.

Figure A.2(b) shows an instant of time in the range $0 < t < \frac{L_1}{c_o}$. The particle velocity on the left side of bar 1 is still V_1, but it has been reduced by half over the rest of the length. The left end of bar 2 also has velocity of $\frac{V_1}{2}$. Note also that a rectangular compressive stress pulse of magnitude $\frac{EV_1}{2c_o}$ has developed on the right part of bar 1 and on the left of bar 2. The arrows indicate the direction of motion of the fronts.

Figure A.2(c) shows an instant of time in the range $\frac{L_1}{c_o} < t < \frac{2L_1}{c_o}$. At this time the particle speed on the left side of bar 1 has become zero and so has the stress. The particle velocity over the rest of the striker bar and the left segment of the transmission bar is $\frac{V_1}{2}$. The magnitude of the compressive stress pulse over the same segments is still $\frac{EV_1}{2c_o}$.

Finally, Fig. A.2(d) shows states with $t > \frac{2L_1}{c_o}$. At this time the particle velocity and the stress are zero everywhere in bar 1, indicating that it has come to rest and is unloaded. A rectangular pulse of particle velocity $\frac{V_1}{2}$ and compressive stress magnitude $\frac{EV_1}{2c_o}$ now travels down the transmission bar. The length of the pulse is $2L_1$.

In summary, the final result of the bar impact described here is a rectangular compressive stress pulse traveling to the right on the semi-infinte bar, while the striker bar is at rest and unloaded.

Transmission and Reflection Across an Impedance Mismatch

Consider a stress pulse σ_i that impinges on a discontinuity in the bar as shown in Fig. A.3. This gives rise to a reflected pulse with stress σ_r and a transmitted pulse with stress σ_t.

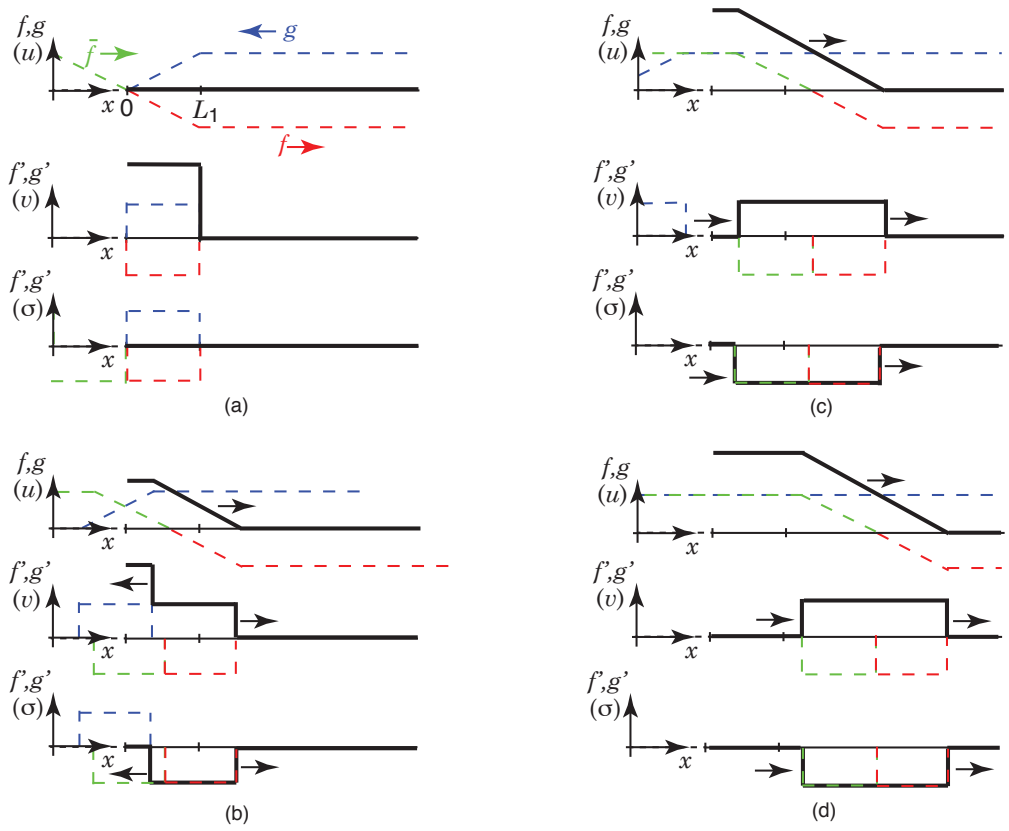

Figure A.2. Schematic showing the impact between a bar of length L_1 moving to the right with a semi-infinite bar. Qualitative resultants for displacement, particle velocity and stress are shown in thick line, and the arrows indicate the direction of motion of the fronts. (a) At the instant of impact, $t = 0$, (b) $0 < t < \frac{L_1}{c_o}$, (c) $\frac{L_1}{c_o} < t < \frac{2L_1}{c_o}$ and (d) $t > \frac{2L_1}{c_o}$

.

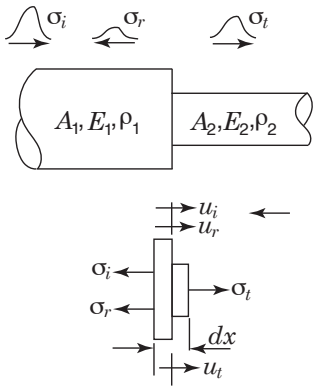

Figure A.3. Wave transmission and reflection across a discontinuity.

Using the equation of motion at the discontinuity and letting $dx \to 0$ gives

$$(\sigma_i + \sigma_r)A_1 = \sigma_t A_2. \tag{24}$$

Enforcing displacement compatibility at the discontinuity gives

$$u_i + u_r = u_t. \tag{25}$$

Taking one derivative with respect to time gives

$$v_i + v_r = v_t, \tag{26}$$

which using (5) and (7) can be rewritten as

$$-c_1\frac{\sigma_i}{E_1} + c_1\frac{\sigma_r}{E_1} = -c_2\frac{\sigma_t}{E_2}. \tag{27}$$

Taking σ_i as known, (24) and (27) represent a system of two equations for two unknowns as follows:

$$\begin{aligned} \sigma_r A_1 - \sigma_t A_2 &= -\sigma_i A_1 \\ \frac{c_1}{E_1}\sigma_r + \frac{c_2}{E_2}\sigma_t &= \frac{c_1}{E_1}\sigma_i. \end{aligned} \tag{28}$$

The solution is:

$$\sigma_r = \frac{A_2\rho_2 c_2 - A_1\rho_1 c_1}{A_1\rho_1 c_1 + A_2\rho_2 c_2}\sigma_i \tag{29}$$

$$\sigma_t = \frac{2A_1c_2\rho_2}{A_1\rho_1c_1 + A_2\rho_2c_2}\sigma_i.$$

Note that σ_r and σ_t have the same shape as σ_i but are scaled depending on the characteristics of the bars on either side of the discontinuity. In particular, note that if $A_2 = E_2 = \rho_2 = 0$, the equations yield $\sigma_r = -\sigma_i$ as expected from a free end. On the other hand, if $A_2\rho_2E_2 \to \infty$, then $\sigma_r = \sigma_i$ which is typically associated with reflection of a wave from a fixed end.

DISTRIBUTION:

1	MS 0557	D. Croessmann, 1520
1	MS 0557	D. Epp, 1522
1	MS 0557	D. Jones, 1558
1	MS 0557	B. Sanborn, 1558
1	MS 0557	B. Song, 1558
1	MS 0815	J. Johannes, 1500
1	MS 0840	J. Redmond, 1550
1	MS 0840	B. Reedlunn, 1554
1	MS 0840	E. Fang, 1554
1	MS 1160	E. Nishida, 5431
1	MS 0899	Technical Library, 9536 (electronic copy)

Sandia National Laboratories